GEOSCIENCE FRONTIERS 3(5) (2012) 669–680

available at www.sciencedirect.com

China University of Geosciences (Beijing)

GEOSCIENCE FRONTIERS

journal homepage: www.elsevier.com/locate/gsf

RESEARCH PAPER

Petrologic characteristics and genesis of dolostone from the Campanian of the SK-I Well Core in the Songliao Basin, China

Xiang Gao [a,b,*], Pingkang Wang [c], Dairong Li [a], Qiang Peng [a], Chengshan Wang [a], Hongwen Ma [b]

[a] *Science Research Institute, China University of Geosciences, Beijing 100083, China*
[b] *National Laboratory of Mineral Materials, China University of Geosciences, Beijing 100083, China*
[c] *Institute of Mineral Resources, Chinese Academy of Geological Sciences, Beijing 100037, China*

Received 2 August 2011; accepted 9 January 2012
Available online 14 January 2012

KEYWORDS
Dolostone;
Genesis;
Cretaceous Nenjiang Formation;
SK-I well core;
The Songliao Basin;
China

Abstract The well SK-I in the Songliao Basin is the first scientific borehole targeting the continental Cretaceous strata in China. Oval concretions, thin laminae and beds of dolostone are found intercalated within mudstone and organic-rich black shale in the Nenjiang Formation of Campanian age. Low ordered ferruginous dolomite is composed of euhedral–subhedral rhombs with cloudy nucleus and light rims formed during the diagenesis, which are typical features of replacement. The heavy carbon isotopes ($\delta^{13}C_{PDB}$ − 1.16–16.0) are results of both the fermentation of organic matter by microbes and degassing of carbon dioxide during the period of diagenesis, and the presence of light oxygen isotopes ($\delta^{18}O_{PDB}$ − 18.53 ~ −5.1) is a characteristic feature of fresh water influence which means the carbonate may have been altered by ground water or rainwater in the late diagenesis. Marine water incursions into the normally lacustrine basin have been proved by both the salinity of *Z* value and the occurrence of foraminifera in the same strata where dolomite occurs. Pyrite framboids observed by SEM are usually enclosed in the dolomite crystals or in the mudstones, supporting the sulfate reducing bacteria (SRB). The formation of both dolomite and pyrite are associated with marine water incursions, which not only supply magnesium

* Corresponding author.
E-mail address: xgao@cugb.edu.cn (X. Gao).

Peer-review under responsibility of China University of Geosciences (Beijing).
doi:10.1016/j.gsf.2011.12.014

ion for dolomite, but also result in limited carbonate precipitation in the basin. The presence of pyrite framboids indicates the development of an anoxic environment associated with salinity stratification in the lake. The dolomite in the Nenjiang Formation is the results of marine water incursions, diagenetic replacement of calcareous carbonate and sulfate reducing bacteria (SRB).

1. Introduction

Dolomite has been extensively studied since it was described for the first time by French naturalist Deodalt de Dolemieu in 1791 (Hardie, 1987; Warren, 2000). It is the ubiquitous component of sedimentary strata from Precambrian to Cenozoic, but volumetrically less represented in younger strata (Given & Wilkinson, 1987; McKenzie, 1991). The major ambiguity of the dolomite formation mechanism is that recently formed dolomite has not yet been found, although "protodolomite" has been reported from Bahamas (Shinn et al., 1965) and Coorong lagoon of Australia (Von Der Borch and Jones, 1976). Stoichiometric dolomite has not yet been synthesized in the laboratory under normal temperature and pressure conditions, and also has not been found precipitated in modern lakes. Thus the question is still open, are all the dolomites formed by secondary replacement, or a part of them remains unchanged? The genetic models proposed for dolomite origin include at least 15 different hypotheses (Jiang, 2003). Therefore, the genesis of dolomite remains wide open and a subject of many sedimentary studies.

The Songliao Basin in northeast China is one of the largest Cretaceous continental rift basins in the world, and the largest oil-bearing basin in China. Dark mudstone in the Nenjiang Formation is one of the most important oil production layers, and it occurs interbedded with thin layer dolostone. However, the genesis of dolostone has been unclear since the basin was explored in 1950's (Yang et al., 1985). Studying the characteristics of dolostone formed in the Nenjiang Formation has a great significance in understanding the paleo-environment and the formation mechanism of petroleum.

2. Geological setting and sample description

The SK-I well with two drillings (south and north) is located in the Qijia-Gulong Sag which is one of the deposition centers of the Songliao Basin, northeast of China (Fig. 1). The basin is of rift origin, infilled with mainly lacustrine sedimentary strata of Cretaceous age, and deposited in moderate-deep to deep lake environments. The lacustrine dolostone are mainly found in the first and second members of the Nenjiang Formation in SK-I(s), Campanian in age (Jilin, 1993).

The well core of the dark mudstone encloses thin laminae and oval concretions of dolostone, limestone, small amount of siltstone, muddy siltstone and silty mudstone. Dolostone occurs as layers of few millimeters to several centimeters thick, which are interbedded with mudstone. The boundaries between dolostone layers and surrounding mudstone are sharp. Dolostone as oval shape concretions embedded within the mudstone are of small size (<5 mm). Both lithologies are found intercalated within dark mudstone and organic-rich black shale of the Nenjiang Formation. Because thin dolostone layers are always interbedded with mudstone, it is rather difficult to separate pure dolostone from mudstone. Therefore, only 15 samples were collected from the core of the first member of the Nenjiang Formation in SK-I(s), including 7 pure dolostone, 4 pure limestone and 4 mudstone samples (see Table 1). Distribution of the 11 carbonate samples is shown in Fig. 2. It shows that carbonate samples are mainly from layers, only two samples are from oval concretions.

3. Experimental methods and conditions

X-ray diffraction (XRD) was performed in the X-ray Laboratory of the China University of Geosciences, Beijing, on the D/Max-RC Powder Diffractometer (Rigaku). The experimental conditions are: Cukα1, graphite monochromator, scintillation counter, voltage at 40 kV, current at 80 mA, continuous scan, slit system DS = SS = 1°, and RS = 0.15 mm. Samples were ground into 300 mesh grains in agate bowl, packed in glass indentation, and pressed into plate type. The scan range is 3–70° 2θ, and scan speed is 8°/min.

The main chemical elements were analyzed in the Electron Probe Laboratory, Chinese Academy of Geological Sciences, Beijing, using a JXA-8800R Electron Probe. Experimental conditions are: voltage at 20 kV, current at 20 mA, spot diameter 5 μm. Samples were polished into smooth face, and sprayed with carbon for measurement.

The trace elements and rare earth elements were measured in the Laser Plasma Laboratory, China University of Geosciences, Beijing, using an Agilent 7500 plasma mass spectrometer (ICP-MS). The standard sample AGV2 from the United States Geological Survey was used, and the rock samples R1 and R2 from the National Research Center of Geological Analysis, China were used for quality control during the analysis. The experimental error is in the range of 10%–15% for Ni, Co, Cr, Sc and <10% for other elements.

Carbon and oxygen stable isotopes were analyzed in the Isotope Laboratory of China University of Geosciences, Beijing, using a MAT253 gaseous isotopic spectrometer. Phosphoric acid method was used, and the environmental conditions are temperature at 22 °C and humidity of 30%. Constant temperature reaction is at 90 °C for 2 h. The size of sample grains is about 74 μm, and analytical precision is ±0.2‰.

Scanning electron microscopic (SEM) analysis was performed in the Physics College of Peking University, and the Key Laboratory of Continental Dynamics, Chinese Academy of Geological Sciences. The apparatus are Amray 1910FE scanning electron microscope at Peking University and JSM-5610LV SEM of Japanese JEOL with INCA energy dispersive spectrometer (EDS) of British Oxford Company in Chinese Academy of Geological Sciences. The accelerating voltage is 20 kV, the focusing distance is 20 mm, and the beam diameter is 40 nm. Pure metal Co is used to optimize the EDS system. The EDS method was used to analyze chemical elements of the mineral. To improve the imaging performance, the fresh faces of cross sections were coated with carbon for testing.

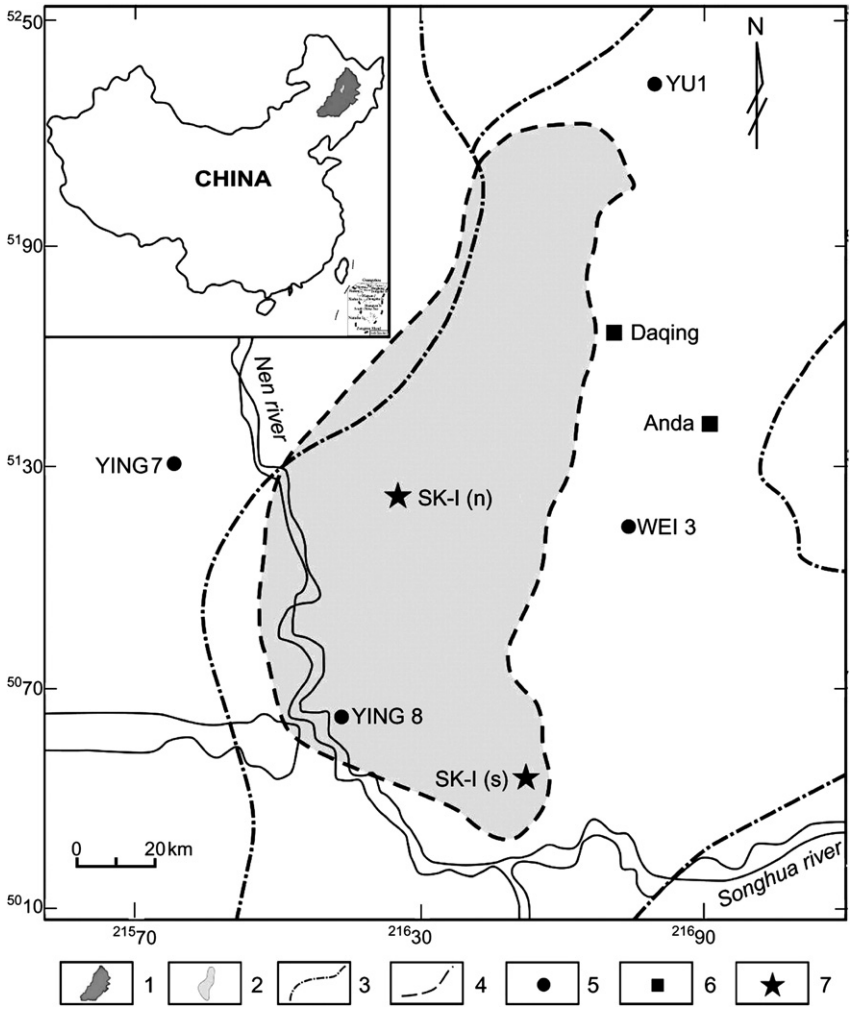

Figure 1 The location of well SK-I with two drillings.
(Note: 1. The Songliao Basin; 2. The Qijia-Gulong Sag; 3. The first grade of the boundary for sag; 4. The second grade of the boundary for sag; 5. Location of other wells; 6. Name of city nearby; 7. Location of well SK-I.)

Table 1 Description of tested samples from the SK-I(s) well core.

Sample Nos.	Depth (m)	Structure	Color	Lithology	Test methods				
					RM	SEM	XRD	EPMA	C-O isotope
S-N1-2	1024.5	Layer	Black	Mudstone	√	√	√	-	-
S-N1-5	1036.78	Layer	Pale olive gray	Microcrystal dolostone	√	√	√	√	√
S-N1-9	1043.13	Oval concretion	Pale olive gray	Microcrystal dolostone	√	√	√	√	√
S-N1-11	1047.18	Layer	Black	Mudstone	√	√	√	-	-
S-N1-13	1048.74	Oval concretion	Pale olive gray	Microcrystal dolostone	√	√	√	√	√
S-N1-23	1053.71	Layer	Olive gray	Microcrystal dolostone	√	√	√	√	√
S-N1-24	1058.99	Layer	Olive gray	Microcrystal dolostone	√	√	√	√	√
S-N1-30	1063.95	Layer	Pale gray	Microcrystal dolostone	√	√	√	√	√
S-N1-33	1067.19	Layer	Black	Mudstone	√	√	√	-	-
S-N1-34	1067.89	Layer	Black	Mudstone	√	√	√	-	-
S-N1-36	1068.69	Layer	Pale gray	Microcrystal dolostone	√	√	√	√	√
S-N1-39	1070.76	Layer	Gray	Microcrystal dolostone	√	√	√	√	√
S-N1-53	1094.64	Layer	Gray	Finecrystal limestone	√	√	√	√	√
S-N1-56	1097.12	Layer	Pale gray	Microcrystal dolostone	√	√	√	√	√
S-N1-57	1098.12	Layer	Pale gray	Microcrystal dolostone	√	√	√	√	√

(Note: RM = Reflecting microscope; SEM = Scanning Electron Microscopic; EPMA = Electron Probe Micro-Analyzer).

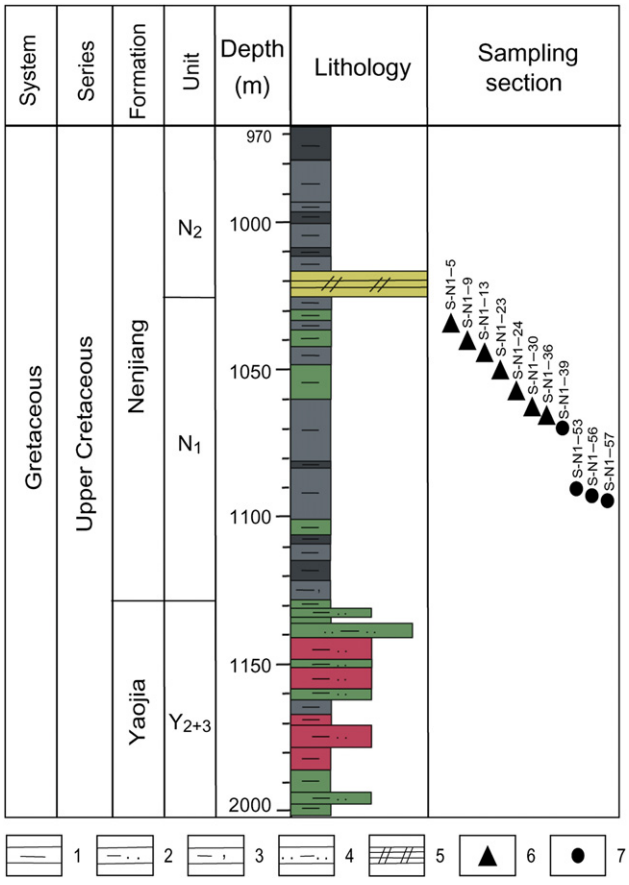

Figure 2 Lithology and sample locations of the carbonates in the first member of the Nenjiang Formation from SK-I(s) borehole. (Note: 1. mudstone; 2. silty mudstone; 3. mud including ostracods; 4. muddy siltstone; 5. oil shale; 6. samples position of dolostone; 7. samples position of limestone.)

4. Characteristics of dolostone

4.1. Microscopic mineralogy and X-ray diffraction

The texture and mineralogy of dolostone were investigated by optical microscope, SEM and XRD, respectively.

4.1.1. Dolomite texture

The dolomite under optical microscope has microlitic structure (Fig. 3A), with crystals of euhedral–subhedral shape (Fig. 3B). Under SEM, the dolomite crystals show rhombohedron of euhedral–subhedral shape, with light rims and dark centers. The particles aggregate in a cumulative texture (see Fig. 4A, B). The space between dolomite crystals is filled by layered clay minerals, which from XRD analysis (see Fig. 5), are illite, illite/smectite mixed layer (I/S) and kaolinite.

4.1.2. The degree of order for dolomite in crystal structure

In a well ordered dolomite crystal, $CaCO_3$ layer and $MgCO_3$ layer alternate regularly, which defines a well ordered crystal structure, with the order being 1. Generally, dolomite is not an ideal crystal, and the intensity ratio of (015) and (110) diffraction peaks indicates approximately the degree of order in the crystal structure: $\triangle = I_{(015)}/I_{(110)}$, where $\triangle$ is the degree of order, I is the intensity of diffraction peak. If the ratio is close to 1, then the degree of order is high. Furthermore, molar content of $CaCO_3$ in the dolomite can be calculated approximately by the formula: $N_{CaCO3} = M\ d_{(104)} + B$, Where N_{CaCO3} represents $CaCO_3$ molar fraction in the crystal lattice of dolomite, $d_{(104)}$ is the d-spacing of the strongest peak (104). M and B are constants, M = 333.33, B = −911.11 (Lindholm, 1987).

XRD results of 7 dolostone samples show that the main mineral is dolomite, with minor amounts of quartz and kaolinite (see Fig. 6). In addition, the degree of order and the $CaCO_3$ molar content of dolomite in the crystal lattice are calculated (see Table 2). The ordered degree are in the range of 0.324–0.643, with an average value of 0.426; $CaCO_3$ molar content are in the range of 52.21–59.55 g/molar, with an average 54.31 g/molar. The lower ordered degree and calcium-rich composition indicate that the mineral was formed by replacing part of Ca^{2+} in calcium carbonate with Mg^{2+} and minor Fe^{2+} during precipitation.

4.2. Geochemical characteristics

The results of major, trace and rare earth element chemistry, and C-O isotopes of the dolostones are briefly discussed below.

4.2.1. Major elements

The composition of dolomite is shown in Table 3. CaO and MgO are the main components, comprising 45.82%–51.87%; the

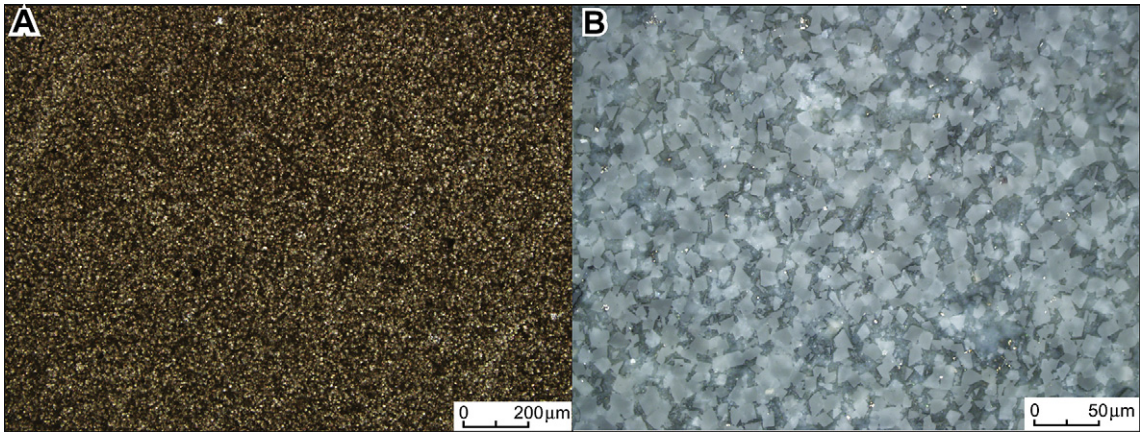

Figure 3 Petrographic features of the microcrystal dolomite. A: microlitic structure, crossed nicols, 10 × 10 μm; B: Rhombus euhedral crystals of dolomite, reflect nicols, 10 × 40 μm.

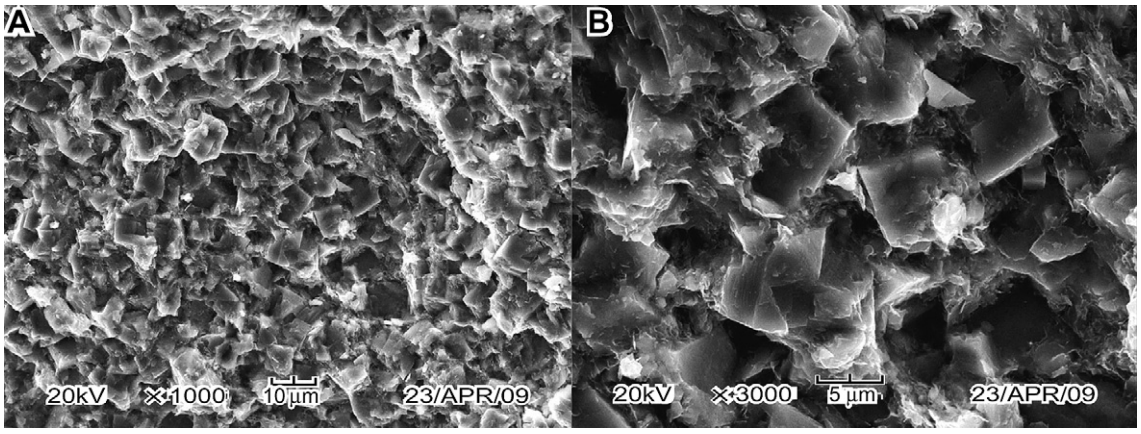

Figure 4 SEM features of the microcrystal dolomite. A: Crystals aggregate in a cumulative texture; B: Rhombus euhedral–subhedral shapes, having structure of cloudy centers and light rims. Clay minerals with layer structure exist in dolomite.

secondary components are FeO_T and SiO_2, FeO_T in range of 2.12%–4.70%, and SiO_2 0.71%–2.57%; small amount of components are Na_2O, Al_2O_3, and MnO, in range of 0.08%–0.41%. Other rare components are K_2O, TiO_2, Cr_2O_3, P_2O_5 and NiO. The remaining is assumed to be CO_2 because light elements cannot be detected by the Electron Probe.

Combined with XRD phase analysis results (see Fig. 6), the SiO_2 is from quartz and kaolinite, whereas CaO, MgO and FeO_T come from the dolomite. However, the content of MgO is higher than that of FeO_T in dolomite, thus according to the composition (Wang et al., 1987), it should be named ferruginous dolomite rather than ankerite as suggested by previous researchers (Liu and Wang, 1997; Wang et al., 2008).

4.2.2. Trace elements and rare earth elements

The results of trace and rare earth elements composition in dolostone of the Nenjiang Formation are summarized in Table 4. The distributions of trace elements in the five dolomite samples are similar (Fig. 7). The highest is the Mn content of 1087–2212 ppm; followed by Sr, Ti and Ba of 678.8–978.6 ppm, 318.2–956.8 ppm and 231.7–374.7 ppm, respectively; with other elements having contents lower than 100 ppm. The Sr/Ba values are in the range of 1.81–4.21, with an average value of 3.03. As Sr/Ba value is higher than 1, it indicates that the origin could be the sedimentary environment of a saline lake or marine (Liu, 1984). The REE pattern is relatively flat, decreasing to the right (Fig. 8), with $\Sigma LREE > \Sigma HREE$, having a strong negative Eu abnormal.

4.2.3. C-O stable isotopes

The C-O stable isotopes results of carbonates are summarized in Table 5. Carbonate samples show presence of heavy carbon isotope ($\delta^{13}C_{PDB}$ − 1.16～16.0) and light oxygen ($\delta^{18}O_{PDB}$ − 18.53～−5.1). Presence of light oxygen isotopes in carbonate is

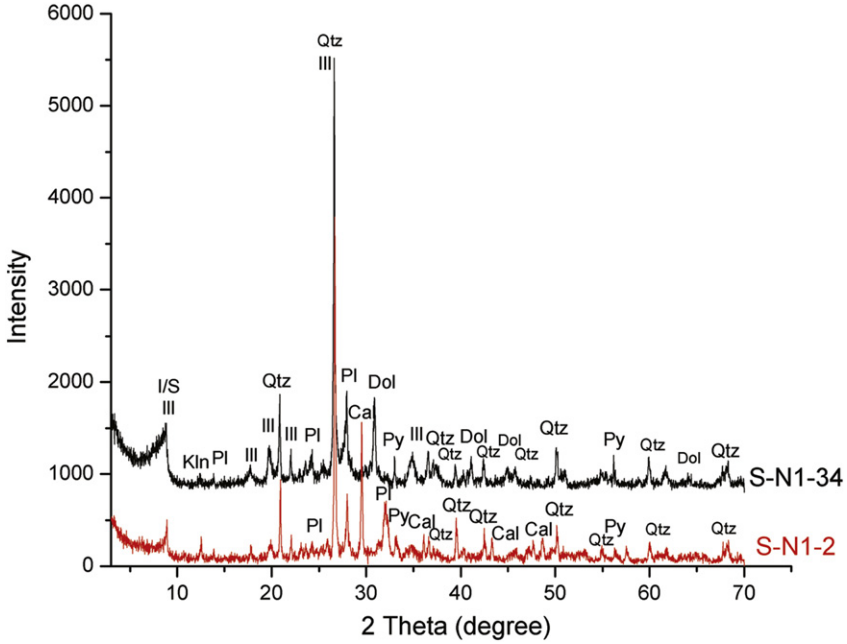

Figure 5 XRD patterns of mudstone samples. I/S – Illite/smectite mixed layer, Ill – Illite, Kln – Kaolinite, Qtz – Quartz, Pl – Plagioclase, Dol – Dolomite, Cal – Calcite, Py – Pyrite.

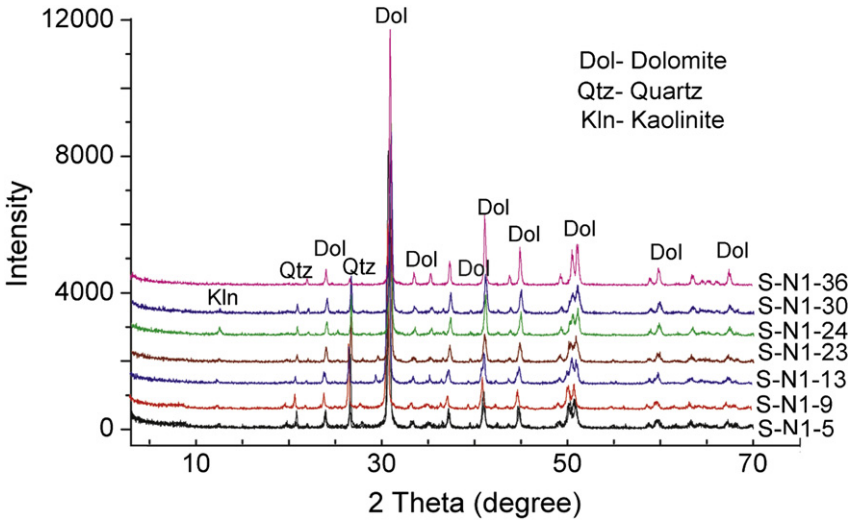

Figure 6 XRD patterns for dolostone samples.

Table 2 The degree of order and $CaCO_3$ molar content of dolostone by XRD analysis.

Sample nos.	Well depth (m)	$d_{(104)}$ (Å)	$I_{(015)}$	$I_{(110)}$	Degree of order(△)	N_{CaCO3} (g/molar)
S-N1-5	1041.03	2.912	143	383	0.373	59.55
S-N1-9	1043.13	2.899	150	354	0.424	55.21
S-N1-13	1048.74	2.890	198	308	0.643	52.21
S-N1-23	1053.71	2.901	134	395	0.339	55.88
S-N1-24	1058.99	2.890	194	438	0.443	52.21
S-N1-30	1063.95	2.892	167	515	0.324	52.88
S-N1-36	1068.69	2.890	354	809	0.438	52.21

a characteristic feature of fresh water influence, indicating that the carbonate may have been altered by ground water or rainwater during late diagenesis (Zhang, 1997). Heavy carbon – $\delta^{13}C_{PDB}$ in samples could be the result of fermentation of organic carbon in an anoxic environment (Irvin et al., 1977). However, when compared with the limestone, dolostone has more heavy carbons, indicating higher salinity of fluids water and stronger reducing environment. It is the contribution from both organic matter decomposed by bacteria and degassing of carbon dioxide which result in accumulated heavy carbons being preserved in a strong reducing environment (Talbot, 1990; Valero-Garces and Emilto, 1995; Mees et al., 1998; Schwalb et al., 1999). $\delta^{18}O_{PDB}$ in dolomite is

Table 3 Major elements in the dolomite samples by EPMA analysis (w_B(%)).

Components	Sample Nos.						
	S-N1-5 (3)	S-N1-9 (3)	S-N1-13 (5)	S-N1-23 (3)	S-N1-24 (6)	S-N1-30 (3)	S-N1-36 (5)
CaO	29.67	34.02	27.91	30.65	29.03	29.13	28.21
MgO	18.10	17.85	17.91	19.78	17.78	17.36	19.51
FeO_T	3.25	2.70	4.70	3.33	4.13	4.48	2.12
SiO_2	2.57	1.45	1.43	0.89	0.71	1.54	1.14
Na_2O	0.13	0.17	0.09	0.12	0.08	0.13	0.10
Al_2O_3	0.41	0.41	0.27	0.34	0.17	0.40	0.27
MnO	0.11	0.11	0.21	0.14	0.11	0.15	0.16
K_2O	0.06	0.06	0.08	0.06	0.04	0.07	0.05
TiO_2	0.01	0.04	0.01	0.02	0.21	0.03	0.03
Cr_2O_3	0.01	0.00	0.03	0.03	0.03	0.01	0.01
P_2O_5	0.06	0.05	0.10	0.08	0.09	0.09	0.12
NiO	0.01	0.01	0.01	0.01	0.01	0.01	0.01
Total	54.39	56.87	52.74	55.45	52.39	53.40	51.73

(Note: (*n*) represents spot numbers tested by EPMA. FeO_T means total ferroan contents.)

Table 4 Trace and rare elements for dolostone samples (values in ppm).

Elements	Sample Nos.				
	S-N1-9	S-N1-13	S-N1-23	S-N1-30	S-N1-36
Li	30.03	25.20	27.20	25.87	11.76
Sc	11.91	10.44	10.59	7.648	2.290
Ti	956.8	379.0	533.9	586.9	318.2
V	63.28	55.47	70.43	63.05	52.20
Cr	23.88	13.37	17.40	15.24	8.391
Mn	1937	2011	2212	1431	1087
Co	2.956	3.365	2.232	3.459	1.530
Ni	6.588	5.230	4.581	6.316	3.707
Cu	13.37	6.568	5.615	7.175	7.026
Zn	29.88	23.86	29.88	26.69	25.49
Ga	6.311	2.446	2.985	3.163	1.424
Rb	37.66	13.31	15.72	17.56	8.722
Sr	678.8	978.6	768.9	936.8	964.7
Y	21.54	9.212	18.30	11.97	5.143
Zr	59.58	38.76	63.85	77.70	73.22
Nb	3.830	1.421	1.949	2.128	1.277
Cs	2.956	1.069	1.240	1.448	0.782
Ba	374.7	232.5	337.0	350.0	231.7
Hf	1.299	0.524	0.749	0.819	0.670
Ta	0.206	0.074	0.104	0.105	0.117
Pb	4.534	3.735	3.228	6.560	5.915
Th	4.028	1.372	1.653	1.974	1.158
U	2.965	1.139	1.316	1.043	0.590
Sr/Ba	1.81	4.21	2.28	2.68	4.16
La	21.56	8.342	9.938	9.398	5.946
Ce	43.18	17.35	21.86	19.50	12.37
Pr	5.256	1.945	2.582	2.276	1.373
Nd	19.97	7.324	10.40	8.726	4.938
Sm	4.116	1.504	2.346	1.877	0.960
Eu	0.800	0.310	0.497	0.383	0.247
Gd	3.902	1.465	2.476	1.899	0.898
Tb	0.596	0.222	0.409	0.290	0.135
Dy	3.532	1.444	2.646	1.801	0.784
Ho	0.731	0.310	0.595	0.390	0.157
Er	2.098	0.935	1.833	1.169	0.443
Tm	0.315	0.148	0.285	0.179	0.064
Yb	1.972	0.998	1.885	1.206	0.411
Lu	0.302	0.166	0.294	0.202	0.067
ΣLREE	94.882	36.775	47.623	42.16	25.834
ΣHREE	13.448	5.688	10.423	7.519	3.206

slightly higher than in the limestone, indicating the difference in original source. Sample S-N_1-53 has abnormal C-O isotope value ($\delta^{13}C_{PDB}$ − 1.16, $\delta^{18}O_{PDB}$ − 18.53) which may be due to the influence of fluids rich in organic matter during diagenesis.

The paleo-salinity in water can be inferred from the Z value (Keith & Weber, 1964), calculated according to the formula: $Z = 2.048(\delta^{13}C_{PDB} + 50) + 0.498(\delta^{18}O_{PDB} + 50)$. If $Z < 120$, it indicates a freshwater environment; if $Z > 120$, it indicates a marine environment, or the participation of sea water during precipitation. Table 5 shows that the Z value for dolostone is ranging between 126 and 157, with an average value of 143; and for limestone, Z value is in the range of 116–123, with an average value of 121. Z value of all carbonate samples is higher than 120, which indicate the influence of sea water in the dolomite formation in the first member of the Nenjiang Formation. One support for the paleo-salinity calculation of dolomite is the occurrence of both benthic and planktonic foraminifera at depth from 1005.62 m to 1123.62 m, which is the stratigraphic level where dolostone occurs. This is a direct evidence for marine water incursions into the Songliao Basin during deposition of the Lower Nenjiang Formation (Xi et al., 2011). As dolostone are missing in other lacustrine sedimentary strata in the basin, it is concluded that the sea water provided Mg^{2+} source for the formation of dolomite. Therefore, marine water incursions may play an important role in formation of dolomite in the Nenjiang Formation.

5. Pyrite

Pyrite (FeS_2), a common sulfide mineral in sedimentary rocks, can be formed in hydrothermal environment, low-temperature

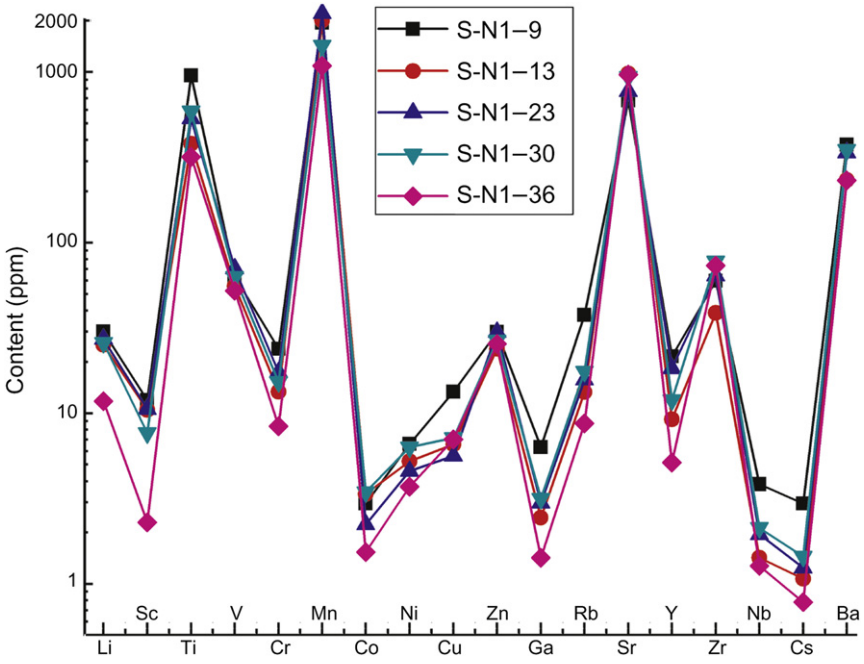

Figure 7 Trends of trace elements in the dolostone samples.

diagenetic environment or precipitate in anoxic waters. It is a typical mineral found in organic-rich sediments and also an indicator of euxinic depositional conditions (Davis et al., 1988; Wilkin et al., 1996; Wang and Morse, 1996; Wilkin and Barnes, 1997; Wignall and Newton, 1998; Wilkin and Arthur, 2001; Schoonen, 2004; Wignall et al., 2005; Shen et al., 2007; Zhou and Jiang, 2009). Pyrite is widely distributed in the first member of the Nenjiang Formation where dolomite is present.

XRD results show that the mudstone interbedded with dolomite layers is mainly composed of quartz, plagioclase, dolomite, calcite, illite and illite/smectite mixed layer, and also minor pyrite is being pervasively scattered in the rocks (see Fig. 5). As the presence of pyrite indicates reducing deposition conditions, we are interested in finding out whether its origin has been influenced by microbe's activity. Therefore, we conducted a SEM study of pyrite in the dolostone and in the mudstone samples (Figs. 9 and 10).

In the dolostone, pyrite framboids scatter among the rhombic dolomite crystals. They have cubic crystal form, with grain size of about 0.5 μm (Fig. 9). In the mudstone, pyrite crystals are found mainly within ostracod shells, where they have cubic shape, pentagonal dodecahedron or octahedron (Fig. 10A). Single framboids with cubic shape are also present (Fig. 10B). Framboids can aggregate into framboidal aggregates (Fig. 10C), and EDS results show that the main chemical elements of framboids are Fe and S (see Fig. 10C inset), confirming that they are pyrite. In samples we studied, the spheric aggregates of pyrite framboids are the main morphological feature of pyrite.

The term, "framboid" was used in French language for the first time by Rust (1935), and was described as "spherical aggregate of equal granular micron-size pyrite crystals" (Love and Amstutz, 1966; Rickard, 1970). Later, scientists found that pyrite framboids pervasively exists in modern marine sediments, freshwater

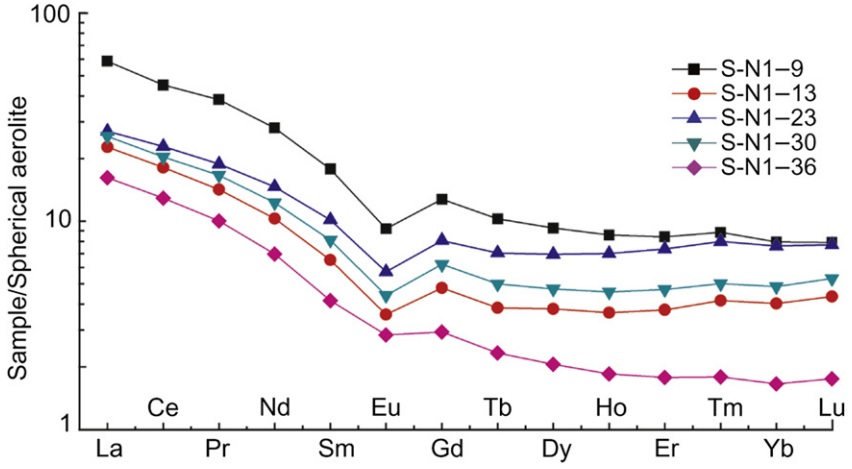

Figure 8 Distribution patterns of rare earth elements in the dolostone samples. (According to aerolite standard value of Taylor and McLennan, 1985).

Table 5 The C-O isotope results of carbonate samples.

Sample nos.	Depth (m)	$\delta^{13}C_{PDB}$ (‰)	$\delta^{18}O_{PDB}$ (‰)	$\delta^{18}O_{SMOW}$ (‰)	Z value
S-N1-5	1036.78	9.1	−7.9	21.36	142
S-N1-9	1043.13	2.00	−11.20	17.96	126
S-N1-13	1048.74	10.3	−8.8	20.44	144
S-N1-23	1053.71	10.7	−8.9	20.33	145
S-N1-24	1058.99	10.4	−7.2	22.08	145
S-N1-30	1063.95	9.67	−8.12	21.14	143
S-N1-36	1068.69	16.0	−5.1	24.25	157
S-N1-39	1070.76	0.75	−11.43	19.07	123
S-N1-53	1094.64	−1.16	−18.53	11.76	116
S-N1-56	1097.12	0.34	−9.48	21.08	123
S-N1-57	1098.12	0.29	−9.15	21.43	123

Note: S-N1-39, 53, 56, 57 are limestone, others are dolostone.

sediments, lacustrine sediments, salt marshes, coal beds, carbonate rocks, moraine sediments, etc. (Stene, 1979; Luther et al., 1982; Weise and Fyfe, 1986; Sassano and Schrijver, 1989; Marnette et al., 1993). It has been suggested that the origin of pyrite framboids is mediated by sulfate reducing bacteria (SRB) activity (Schneiderhöhn, 1923; Love, 1957). This process can be expressed by following equations (Vasconcelos and McKenzie, 1997; Boetius et al., 2000; Orphan et al., 2001):

$$2CH_2O + MgSO_4 \rightarrow H_2S + 2HCO_3 + Mg^{2+} \quad (1)$$

$$2H_2S + Fe^{2+} \rightarrow FeS_2 + 4H^+ \quad (2)$$

Equation (1) shows that the magnesium sulfate is deoxidized into H_2S by SRB with organic matter acting as reductant and energy source under anoxic condition, and in equation (2) H_2S reacted with Fe^{2+}, and eventually pyrite is formed and preserved in the sediments (Berner, 1984; Berner and Raiswell, 1984).

These chemical reactions indicate that the sulfate reduction by microbes will reduce organic matter, and decrease the concentration of sulfate in fluid, thereby reduce the chemical barrier kinetics of sulfate during dolomite precipitation (Baker and Kastner, 1981). In addition, the sulfate in the sea water often exists in the forms of Mg^{2+} and SO_4^{2-}. While the sulfate reducing bacteria consumes sulfate, it can release Mg^{2+} which is a necessary ion for precipitation of dolomite (Vasconcelos and McKenzie, 1997). SEM results of pyrite micro-morphology show that pyrite framboids are enclosed within the rhombs of ferruginous dolomite, confirming that SRB not only supplied the main Mg^{2+} source, but also overcome constraint of chemical kinetics to provide a favorable micro-environment for the formation of ferruginous dolomite. Therefore, we infer that the formation of dolomite in the Cretaceous Nenjiang Formation in the Songliao Basin has been influenced by SRB.

6. Origin of dolomite

The problem of the origin of dolostone has long occupied the minds of geologists, and the controversial aspects of dolomite research are the various models for dolomitization. Furthermore, the genesis of dolostone varies from place to place (Machel, 2004). For this reason, dolostone coming from different places should have to be investigated individually.

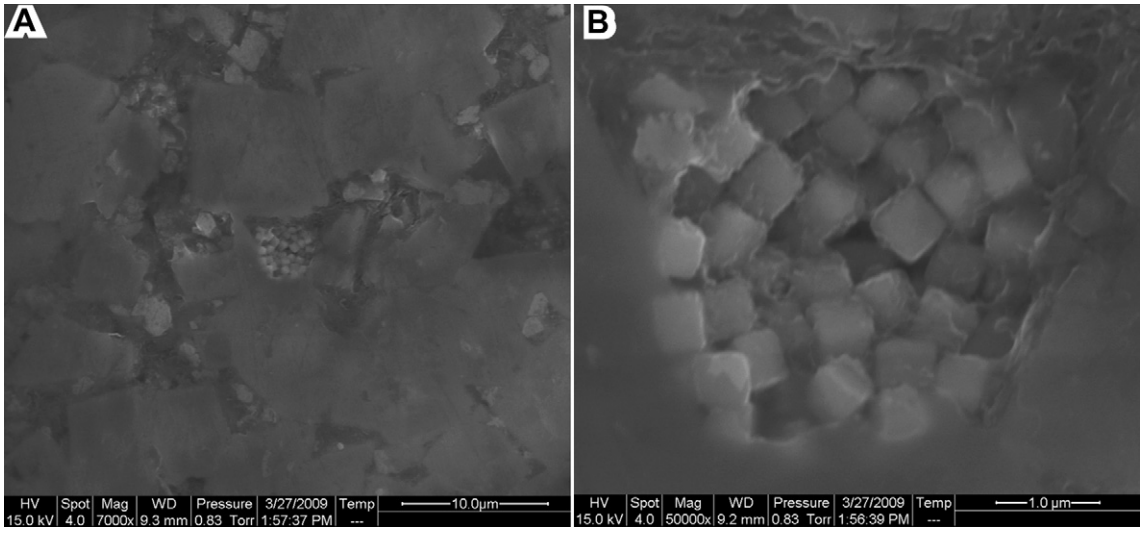

Figure 9 SEM morphology of framboidal pyrite in dolostone. A: Single framboidal pyrite (cubic granule) distributed among the rhombus dolomite crystals; B: Local magnification of Fig. 9A.

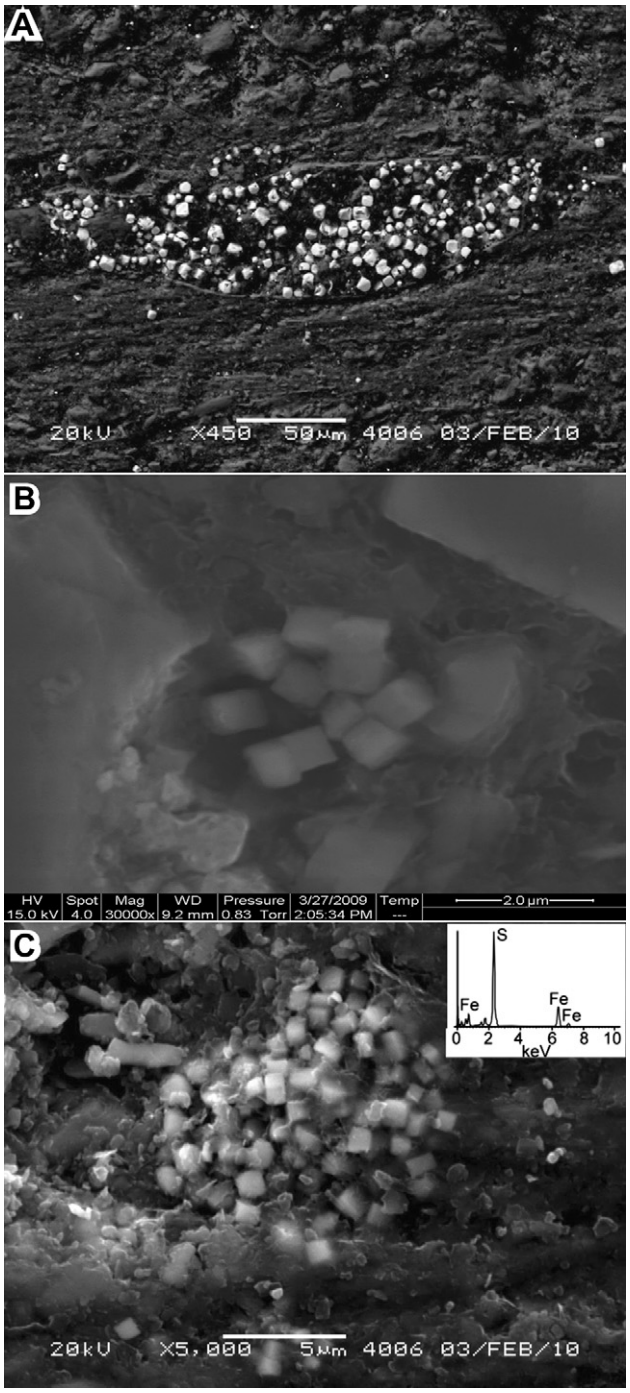

Figure 10 SEM morphology of pyrite in mudrock. A: Euhedral crystal aggregation in biological shell feature; B: Single framboidal pyrite; C: Aggregation of framboidal pyrite scattered in clay minerals and its EDS pattern.

Therefore, based on the petrologic study, the following three mechanisms contribute to the formation of dolomite in the Nenjiang Formation:

6.1. Replacement of calcite during diagenesis

Observed by the polarized light microscopy and SEM, the dolomite of the Nenjiang Formation shows microlitic structure, with euhedral–subhedral rhombic shape. Dolomite is the result of replacement of calcite by Mg^{2+} as evidenced by the typical structure of crystals with a cloudy nucleus and light rims. In addition, the degree of lower order (average value 0.426) and calcium-rich feature (average value 55.48 g/molar) of ferruginous dolomite by XRD also indicate that the mineral formed rapidly in the depositional environment by replacement of Ca^{2+} with Mg^{2+} and minor Fe^{2+}.

6.2. Marine water incursions

Z values of C-O stable isotopes, and higher Sr/Ba values of elements in dolomite reflect the higher salinity in the depositional environment. A contribution from the sea water in the first member of the Nenjiang Formation is supported by recently found foraminifera. Marine water incursions not only supplied the main Mg source, but also caused strong salinity stratification in the lake resulting in bottom waters being anoxic. Therefore, marine water incursions were an instrumental ingredient in the formation of dolomite.

6.3. Sulfate reducing bacteria (SRB)

Pyrite framboids being enclosed in dolostone and mudstone in the strata are the result of sulfate reducing bacteria (SRB). In the interface between sediments and water, the sulfate was deoxidized into H_2S by SRB with organic matter as reductant and energy source under the anoxic condition. H_2S further reacted with Fe^{2+}, and eventually pyrite was formed and preserved in the sediments. At the same time, the fermentation of organic matter and degassing of carbon dioxide concentrated heavy carbons, which were preserved in the form of HCO_3^-, and HCO_3^- further combined with Ca^{2+} to form calcium carbonate (calcite or aragonite), then ferruginous dolomite was formed after Mg^{2+} and minor Fe^{2+} replaced calcium carbonate. This is the reason why the $\delta^{13}C$ values are positive. Therefore, marine water incursions were instrumental in the basin for the formation of dolomite and pyrite framboids.

7. Conclusion

From the study of lacustrine to marine (see foraminifera etc.) sedimentary deposits in the first member of the Nenjiang Formation of the Upper Cretaceous, we established that present dolomite is of ferruginous composition ($FeO_T < MgO$) with microlitic structure. SEM observation shows that the mineral occurs as rhombohedron, euhedral–subhedral shape, with replacement diagenetic texture of cloudy nucleus and light rims of the crystals. The dolomite has lower ordered degree in crystal structure. C-O stable isotopes of dolostone show the presence of heavy carbon and light oxygen. Heavy carbon ($\delta^{13}C$) enrichment is due to both the fermentation of organic matter by microbes and degassing of carbon dioxide during the period of diagenesis. The light oxygen $\delta^{18}O$ is a characteristic feature of fresh water influence which may be altered by ground water or rainwater in the late diagenesis. The salinity of *Z* values (>120) and Sr/Ba value (>1) are all indicating the participation of marine water. The salinity of dolostone is higher than that of limestone, indicating that dolomite was formed in a reducing environment created by the strong salinity stratification in the lake.

Pyrite framboids scattered both in dolomite crystals and mudstone resulted by sulfate reducing bacteria (SRB). Marine

ingression provided magnesium cations for dolomite, and also contributed to the creation of an anoxic environment by salinity stratification in the lake.

Therefore, we conclude that the formation of dolostone within first member of the Nenjiang Formation in the Songliao Basin, China, is associated with marine water incursions into the normally lacustrine basin, diagenetic replacement and sulfate reducing bacteria (SRB).

Acknowledgments

This project was financially supported by the National Key Program for Basic Research 973 Project (Grant No. 2006CB701406) of China, and the Opening Research Program of the National Laboratory of Mineral Materials, China University of Geosciences, Beijing (No.07A007). Thanks to Prof. Lubomir Jansa for providing some good suggestions.

References

Baker, P., Kastner, M., 1981. Constraint on the formation of sedimentary dolomite. Science 213, 214–216.

Berner, R.A., 1984. Sedimentary pyrite formation. Geochimica et Cosmochimica Acta 48, 605–615.

Berner, R.A., Raiswell, R., 1984. C/S method for distinguishing freshwater from marine sedimentary rocks. Geology 12, 365–368.

Boetius, A., Ravenschlag, K., Schubert, C.J., Rickert, D., Widdel, F., Gieske, A., Amann, R., Jørgensen, B.B., Witte, U., Pfannkuche, O., 2000. A marine anaerobic consortium apparently mediating anaerobic oxidation of methane. Nature 407, 623–626.

Davis, H.R., Byers, C.W., Dean, W.E., 1988. Pyrite formation in the Lower Cretaceous Mowry Shale: effect of organic matter type and reactive iron content. American Journal of Science 288, 873–890.

Given, R.H., Wilkinson, B.H., 1987. Dolomite abundance and stratigraphic age: constrains on rates and mechanisms of phanerozoic dolostone formation. Journal of Sedimentary Petrology 57, 1068–1078.

Hardie, L.A., 1987. Dolomitization: a critic view of some current view. Journal of Sedimentary Petrology 57, 166–183.

Irvin, H., Curtis, C., Coleman, M., 1977. Isotopic evidence for source of diagenetic carbonates formed during burial of organic-rich sediments. Nature 269, 209–213.

Jiang, Z.X., 2003. Sedimentology. Petroleum Industry Press, Beijing, p. 82 (in Chinese).

Jilin petroleum geology Compilation Group, 1993. Petroleum Geology of China, vol. 2. Petroleum Industry Press, Beijing, pp. 85–86 (in Chinese).

Keith, M.L., Weber, J.N., 1964. Carbon and oxygen isotopic composition of selected limestone and fossils. Geochimica et Cosmochimica Acta 28, 1787–1816.

Lindholm, R.C., 1987. A Practical Approach to Sedimentology. Allen & Unvin, London, p. 279.

Liu, W.Z., Wang, P.J., 1997. Genesis and environmental significance of dolomite concretions from the Nenjiang Formation in the Songliao Basin, Northeastern China. Sedimentary Geology and Tethyan Geology 17 (1), 22–26.

Liu, Y.J., 1984. Elementary Geochemistry. Science Press, Beijing, p. 53 (in Chinese).

Love, L.G., Amstutz, G.C., 1966. Review of microscopic pyrite from the Devonian Chattanooga Shale and Remmelsberg Banderz. Fortschritte der Mineralogie 43, 273–309.

Love, L.G., 1957. Microorganisms and the presence of syngenetic pyrite. Quarterly Journal of the Geological Society of London 113, 429–440.

Luther III, G.W., Giblin, A., Howarth, R.W., Ryans, R.A., 1982. Pyrite and oxidized iron mineral phases formed from pyrite oxidation in salt marsh and estuarine sediments. Geochimica et Cosmochimica Acta 46, 2665–2669.

Machel, H.G., 2004. Concepts and models of dolomitization: a critical reappraisal. In: Braithwaite, C.J.R., Rizzi, G., Darke, G. (Eds.), The Geometry and Petrogenesis of Dolomite Hydrocarbon Reservoirs. Geological Society, Special Publications, London, pp. 7–63.

Marnette, E.C.L., Breemen, N.V., Horduk, K.A., Cappenberg, T.E., 1993. Pyrite formation in two freshwater systems in the Netherlands. Geochimica et Cosmochimica Acta 57, 4165–4177.

McKenzie, J.A., 1991. The dolomite problem: an outstanding controversy. In: Muller, D.W., McKenzie, J.A., Weissert, H. (Eds.), Controversies in Modern Geology: Evolution of Geological Theories in Sedimentology, Earth History and Tectonics. Academic Press, London, pp. 37–54.

Mees, F., Reyes, E., Keppens, E., 1998. Stable isotope chemistry of gaylussite and nahcolite from the deposits of the crater lake at Malha, northern Sudan. Chemical Geology 146, 87–98.

Orphan, V.J., House, C.H., Hinrichs, Kai-Uwe, Mckeegan, K.D., Delong, E.F., 2001. Methane-consuming archaea revealed by directly coupled isotopic and phylogenetic analysis. Science 293 (5529), 484–487.

Rickard, D.T., 1970. The origin of framboids. Lithos 3, 269–293.

Rust, G.W., 1935. Colloidal primary copper ores at Cornwall mines, southeastern Missouri. Journal of Geology 43, 398–426.

Sassano, G.P., Schrijver, K., 1989. Framboidal pyrite: early-diagenetic, late-diagenetic, and hydrothermal occurrences from Acton Vale quarry, Cambro-Ordovician, Quebec. American Journal of Science 289, 167–179.

Schneiderhöhn, H., 1923. Chalkographische Untersuchung des Mansfelder Kupferschiefers. Neues Jahrbuch für Mineralogie. Geologie und Paläeontologie 47, 1–38.

Schoonen, M.A.A., 2004. Mechanisms of sedimentary pyrite formation. Geological Society of American (Special Paper) 379, 117–134.

Schwalb, A., Burns, S.J., Kelts, K., 1999. Holocene environments from stable isotope stratigraphy of ostracods and authigenic carbonate in Chilean Altiplano Lakes. Palaeogeography, Palaeoclimatology, Palaeoecology 148, 153–168.

Shen, W.J., Lin, Y.T., Xu, L., Li, J.F., Wu, Y.S., Sun, Y.G., 2007. Pyrite framboids in the Permian-Triassic boundary section at Meishan, China: evidence for dysoxic deposition. Palaeogeography, Palaeoclimatology, Palaeoecology 253, 323–331.

Shinn, E.A., Ginsburg, R.N., Lloyd, R.M., 1965. Recent supratidal dolomite from Andros Island, Bahamas. Spec. Publ. No. 13. In: Pray, L.C., Murray, R.C. (Eds.), Dolomitization and Limestone Diagenesis SEPM, pp. 112–123.

Stene, L.P., 1979. Polyframboidal pyrite in the tills of southwestern Alberta. Canadian Journal of Earth Sciences 16, 2053–2057.

Talbot, M.R., 1990. A review of the palaeohydrological interpretation of carbon and oxygen isotopic ratios in primary lacustrine carbonates. Chemical Geology 80, 261–279.

Taylor, S.R., McLennan, S.H., 1985. The continental crust: Its composition and evolution. Blackwell, Oxford, p.312.

Valero-Garces, B., Emilto, K.K., 1995. Oxygen and carbon isotope trends and sedimentological evolution of a meromictic and saline lacustrine system: the Holocene Medicine Lake Basin, North American Great Plains, USA. Palaeogeography, Palaeoclimatology, Palaeoecology 17, 253–278.

Vasconcelos, C., McKenzie, J.A., 1997. Microbial mediation of modern dolomite precipitation and diagenesis under anoxic conditions (Lagoa Vermelha, Rio de Janeiro, Brazil). Journal of Sedimentary Research 67, 378–390.

Von Der Borch, C.C., Jones, J.B., 1976. Spherular modern dolomite from the Coorong area, South Australia. Sedimentology 23, 587–591.

Wang, G.D., Cheng, R.H., Wang, P.J., Gao, Y.F., 2008. The forming mechanism of dolostone of Nenjiang Formation in Songliao Basin-example from CCSD-SK-II. Acta Geologica Sinica 82 (1), 48–55 (in Chinese with English abstract).

Wang, P., Pan, Z.L., Weng, L.B., 1987. Systematical Mineralogy. Geology Press, Beijing, p. 265 (in Chinese).

Wang, Q., Morse, J.W., 1996. Pyrite formation under conditions approximating those in anoxic sediments : I. Pathway and morphology. Marine Chemistry 52, 99–121.

Warren, J., 2000. Dolomite: occurrence, evolution and economically important associations. Earth Science Review 52, 1–81.

Weise, R.G., Fyfe, W.S., 1986. Occurrences of iron sulfides in Ohio coals. International Journal of Coal Geology 6, 251–276.

Wignall, P.B., Newton, R., 1998. Pyrite framboid diameter as a measure of oxygen deficiency in ancient mud rocks. American Journal of Science 298, 537–552.

Wignall, P.B., Newton, R., Brookfield, M.E., 2005. Pyrite framboid evidence for oxygen poor deposition during the Permian-Triassic crisis in Kashmir. Palaeogeography, Palaeoclimatology, Palaeoecology 216, 183–188.

Wilkin, R.T., Barnes, H.L., Brantley, S.L., 1996. The size distribution of framboidal pyrite in modern sediments: an indicator of redox conditions. Geochimica et Cosmochimica Acta 60, 3897–3912.

Wilkin, R.T., Barnes, H.L., 1997. Formation processes of framboidal pyrite. Geochimica et Cosmochimica Acta 61, 323–339.

Wilkin, R.T., Arthur, M.A., 2001. Variations in pyrite texture, sulfur isotope composition , and iron systematics in the Black Sea : evidence for Late Pleistocene to Holocene excursions of the O_2-H_2S redox transition. Geochimica et Cosmochimica Acta 65 (9), 1399–1416.

Xi, D.P., Wan, X.Q., Feng, Z.Q., Li, S., Feng, Z.H., Jia, J.Z., Jing, X., Si, W.M., 2011. Discovery of late cretaceous foraminifera in the Songliao Basin: evidence from SK-I and implications for identifying seawater incursions. Chinese Science Bulletin 56 (3), 253–256.

Yang, W.L., Gao, R.Q., Guo, Q.F., Liu, Y.G., 1985. Movement and assemble Characters of continental oil-gas in the Songliao Basin. Technical and Scientific Press of Heilongjiang Province, Haerbin (in Chinese), Vol. 1, p. 6.

Zhang, H.C., 1997. Supergenic Geochemistry Characteristics and Theoretical Basis. Lanzhou University Press, Lanzhou, p. 219 (in Chinese).

Zhou, C.M., Jiang, S.Y., 2009. Palaeoceanographic redox environments for the lower Cambrian Hetang Formation in South China: evidence from pyrite framboids, redox sensitive trace elements, and sponge biota occurrence. Palaeogeography, Palaeoclimatology, Palaeoecology 271, 279–286.